ACS OMEGA

http://pubs.acs.org/journal/acsodf

Article

Preparation and Adsorption Behavior of Ce(III)-MOF for Phosphate and Fluoride Ion Removal from Aqueous Solutions

Mitin Belaye, Abi M. Taddesse,* Endale Teju, Manuel Sanchez-Sanchez, and Jemal M. Yassin*

Cite This: *ACS Omega* 2023, 8, 23860−23869

Read Online

ACCESS | Metrics & More | Article Recommendations | Supporting Information

ABSTRACT: The discharge of inorganic pollutants like phosphate and fluoride is a cause of mounting concern to the world due to the substantial environmental and human health risk. Adsorption is one of the most common and affordable technologies widely utilized for removing inorganic pollutants such as phosphate and fluoride anions. Investigating efficient sorbents for the adsorption of these pollutants is extremely important and challenging. This work aimed at studying the adsorption efficiency of the Ce(III)-BDC metal−organic framework (MOF) for the removal of these anions from an aqueous solution using a batch mode. Powder X-ray diffraction (XRD), Fourier transform infrared (FTIR), thermogravimetric analysis (TGA), Brunauer−Emmett−Teller (BET), and scanning electron microscopy-energy dispersive X-ray analysis (SEM-EDX) techniques evidenced the successful synthesis of Ce(III)-BDC MOF in water as a solvent without any energy input within a short reaction time. The outstanding removal efficiency of phosphate and fluoride was exhibited at an optimized pH (3, 4), adsorbent dose (0.20, 0.35 g), contact time (3, 6 h), agitation speed (120, 100 rpm), and concentration (10, 15 ppm) for each ion, respectively. The experiment on the effect of coexisting ions demonstrated that SO_4^{2-} and PO_4^{3-} ions are the primary interfering ions in phosphate and fluoride adsorption, respectively, while the HCO_3^- and Cl^- ions were found to have interfered less. Furthermore, the isotherm experiment showed that the equilibrium data fitted well with the Langmuir isotherm model and the kinetic data correlated well with the pseudo-second-order model for both ions. The results of thermodynamic parameters such as $\Delta H°$, $\Delta G°$, and $\Delta S°$ evidenced an endothermic and spontaneous process. The regeneration of the adsorbent made using water and NaOH solution showed the easy regeneration of the sorbent Ce(III)-BDC MOF, which can be reused four times, revealing its potential application for the removal of these anions from aqueous environment.

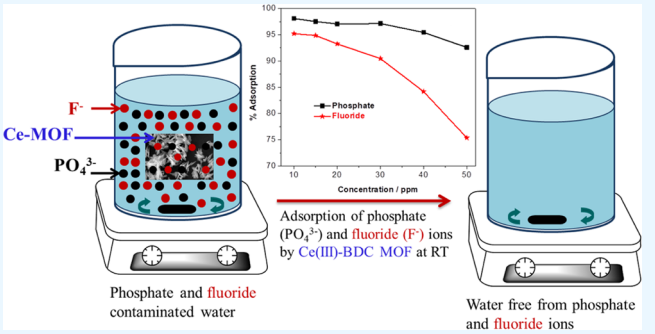

1. INTRODUCTION

Water is among the crucial elements needed for life on the planet, representing the most priceless resource to the present and future societal needs.[1] However, its quality is worsening day by day mainly due to population explosion and as a result of the speedy growth of sectors such as industry and agriculture in addition to geological and environmental pollution of the water bodies (rivers, lakes, seas, and oceans).[2] The standards for drinking water have set maximum allowable limits for various inorganic anions such as phosphate, fluoride, nitrite, nitrate, chloride, arsenate, sulfate, arsenic, cyanide, bromate, etc.[3,4] Among such contaminants, phosphate and fluoride pose substantial risks to the natural environment and are also dangerous to humans at high concentrations.[4−6]

Phosphate is one of the macronutrients required for the growth of plants. Phosphate is released into aqueous environment due to domestic, mining, industrial, agricultural, and municipal activities in inorganic and organic forms.[7] The concentration of phosphate beyond the permissible level in water can cause eutrophication, a major driving force for the growth of aquatic plants, thereby disrupting the ecological balance of the organisms present in water. Eutrophication leads to rapid reduction of dissolved oxygen levels, putting at risk the lives of aquatic animals and plants.[8]

Fluoride contamination in groundwater is a major problem across the globe. The amount of fluoride in drinking water exceeds the maximum permissible level in many areas of the world. The maximum fluoride concentration in natural drinking water should not exceed 1.5 mg L^{-1}. In fact, a certain amount of fluoride (below the maximum permissible level) is essential to humans to prevent dental decay,[9] whereas excessive intake leads to dental and skeletal fluorosis.[10] Therefore, phosphate and fluoride in water sources must be depleted to avoid hazards related to the environment and

Received: April 5, 2023
Accepted: June 2, 2023
Published: June 16, 2023

health. In this regard, there are various methods that are employed for the treatment of wastewater, viz., adsorption,[11] precipitation,[12] ion exchange,[13] and reverse osmosis.[14] Among these, adsorption is the one of the methods employed extensively for the removal of inorganic pollutants because of its ensuing merits such as being an environmentally safe process, simplicity, and low cost. Traditional sorbents such as activated carbons,[15] zeolitic materials,[16] and clay minerals have been used for the removal of anions from wastewater,[17] but they have low sorption capacities and efficiencies that limit their application.

A new form of porous hybrid materials called metal−organic frameworks (MOFs) have attracted significant research interest because of their high surface area, tunable pore structure and composition, high thermal stability, etc.[18−20] Over the past decade, numerous MOFs have been prepared for various applications such as adsorption and storage of gases,[21] environmental remediation,[22,23] sensing,[24] delivery of drugs,[25,26] catalysis,[27,28] and separation.[29,30] Moreover, MOFs are materials with good porosity and reusability, making them amenable for the adsorptive removal of several contaminants from water environment.[31−33]

However, up to now, there is a paucity of information regarding phosphate and fluoride ions' removal from aqueous systems by Ce(III)-BDC MOFs, which is isostructural to lanthanide-BDC MOFs synthesized by hydrothermal (140 °C for 12 h) and urothermal (120 °C for 5 days) approaches with the crystal formula of $M_2(BDC)_6(H_2O)_4$, where M = Tb, Eu, and Ce.[34,35] The objective of this work was, therefore, to fill this gap by assessing the sorption behavior of this MOF considering target pollutants such as phosphate and fluoride ions. Accordingly, Ce(III)-BDC was successfully prepared starting from Ce(III) precursors using a sustainable approach without addition of a modulator, characterized, and various operational parameters (pH, contact time, adsorbent dose, initial adsorbate concentration, agitation speed, and the effect of interfering ions) were optimized. In addition to this, we investigated the isotherm, kinetics, and thermodynamics of the adsorption process.

2. EXPERIMENTAL SECTION

2.1. Materials. Chemicals employed for this work include terephthalic acid (H_2BDC, 98%, Acros Organics), cerium nitrate hexahydrate ($Ce(NO_3)_{324}{\cdot}6H_2O$, 99.5%, Alfa Aesar), ethanol (C_2H_5OH, 99%, BDH Chemicals), potassium dihydrogen phosphate (KH_2PO_4, 99%, BDH Chemicals), ammonium molybdate tetrahydrate ($(NH_4)_6Mo_7O_{24}{\cdot}4H_2O$, 99.3%, Loba Chemie), potassium antimony tartrate trihydrate ($K_2Sb_{224}{\cdot}C_8H_4O_{1224}{\cdot}3H_2O$, 98.5%, Loba Chemie), ascorbic acid ($C_6H_8O_6$, 99%, Sigma-Aldrich), sodium bicarbonate ($NaHCO_3$, 99%, Labkafe), sodium hydroxide (NaOH, 99%, Otto Chemie), sodium fluoride (NaF, 99%, Sigma-Aldrich), sodium chloride (NaCl, 99%, Nice Chemicals), hydrochloric acid (HCl, 37%, Sigma-Aldrich), glacial acetic acid (CH_3COOH, 99.9%, Sigma-Aldrich), and ethylene diamine tetra acetic acid disodium salt (EDTA, 99.5%, Sigma-Aldrich). They were analytical grade and used with no further treatment.

2.2. Preparation of Ce(III)-MOF. Ce(III)-BDC MOF was synthesized in water as a sole solvent by direct precipitation at room temperature,[36] with some modification. Accordingly, 4.34 g of cerium nitrate hexahydrate (10 mmol) and 2.49 g of H_2BDC (15 mmol) were added and dissolved in 30 and 70 mL of deionized water (solution 1 and 2, respectively); the pH of the linker solution was adjusted to 7 by adding the required amount of ammonia solution NH_3/H_2O (V/V = 1:1) under stirring. Then, solution 1 (solution comprising the metal) was poured slowly to solution 2 (solution containing the linker) under vigorous perturbation. Following this, a white product was obtained and stirred continuously for 1 h. The formed precipitate was centrifuged at 3500 rpm for 20 min and the solid was washed with deionized water (four times, ×4), ethanol (×3), and finally dried at 60 °C for 24 h.

2.3. Characterization of the Material. The powder X-ray diffraction (PXRD) pattern was recorded using X'Pert Pro PANalytical equipped with an X-ray source of Cu Kα radiation (λ = 0.15406 nm) at a step scan rate of 0.02 (step time: 1 s) in the 2θ range of 5.0−90.4°. The morphology and composition of the as-synthesized sample were determined by scanning electron microscopy hyphenated with energy dispersive X-ray spectroscopy (SEM-EDX) using a Hitachi Tabletop Microscope TM1000 with a tungsten filament electron gun. The thermal stability of Ce(III)-BDC was studied by a thermogravimetric analysis (TGA) instrument (DTA-60H, DTG, SHIMADZU, Japan), in the temperature range from 20 to 800 °C under N_2 flow. The surface property of Ce(III)-BDC was examined using FTIR (Perkin Elmer) in the range 400−4000 cm^{-1} using the KBr disc method. N_2 sorption isotherms were measured at −196 °C using a Micromeritics Instrument (ASAP 2420) and the specific surface area was estimated by the Brunauer−Emmett−Teller (BET) method.

2.4. Phosphate and Fluoride Adsorption/Removal Experiments. The stock solutions (1000 mg L^{-1}) were prepared by placing appropriate amounts of KH_2PO_4 and NaF in deionized water. The target concentrations of each ion were then determined via serial dilution. Adsorption experiments were conducted in a batch mode using 0.1 g of adsorbent (Ce(III)-BDC MOF) with 25 mL of KH_2PO_4 and NaF solution (20 mg L^{-1}) in separate Erlenmeyer flasks at ambient temperature. The pH of the phosphate and fluoride-containing solutions was adjusted using dilute HCl or NaOH solutions and the experiment was done on a rotary shaker. When the equilibrium was reached, the solution was separated from the adsorbent by filtration, and the final concentration of the unadsorbed phosphate ions was determined using a spectrophotometer by the molybdenum blue method, by fixing the absorbance at 880 nm using an ultraviolet−visible (UV−vis) spectrophotometer (SP65). Similarly, the concentration of the fluoride ions in the solution was determined by ion selective electrodes using TISAB (total ionic strength adjustment buffer). The percentage adsorption and adsorption capacity of the Ce(III)-BDC, for the two analytes considered in the present study, were calculated using the following mathematical relations.

$$\%\ \text{adsorption} = \frac{(C_o - C_e)}{C_o} \times 100 \quad (1)$$

$$\text{adsorption capacity} = (C_o - C_e) \times \frac{V}{m} \quad (2)$$

where C_o and C_e are the initial and equilibrium concentrations of the adsorbate solution (mg L^{-1}), V is the volume of adsorbate solution (mL), and m is the mass of the adsorbent (g).

2.5. Optimization Parameters. The effect of various adsorption parameters on efficient removal of phosphate and fluoride was carefully investigated. The effect of pH was

https://doi.org/10.1021/acsomega.3c02290
ACS Omega 2023, 8, 23860−23869

evaluated by agitating (120 rpm) 0.1 g L^{-1} Ce(III)-BDC MOF with 25 mL of phosphate and fluoride solution (20 mg L^{-1}) at different pH values (2−10) for 24 h. The effect of dose on phosphate and fluoride sorption efficiency was studied by considering the dose in the range from 0.05 to 0.5 g L^{-1} using the optimum pH while keeping the remaining parameters fixed as mentioned above.

To evaluate the contact time effect, time was varied from 1 to 24 h. The adsorption experiment was then executed under the optimized adsorbent dose and pH. The effect of agitation speed was assessed by varying the agitation speed (50, 100, 120, 150, and 200 rpm) for both anions by mixing 25 mL of an initial concentration of 20 mg L^{-1} of both ions keeping the dose, pH, and contact time at their corresponding optimal values. To assess the effect of adsorbate initial concentration, the experiment was conducted using different initial phosphate and fluoride ion concentrations (10, 15, 20, 30, 40, and 50 mg L^{-1}). 0.2 g of phosphate and 0.35 g of fluoride ions of the adsorbent (optimum values) were loaded into a 50 mL Erlenmeyer flask and 25 mL of each of the initial phosphate and fluoride ion solutions was then added, respectively, keeping all other parameters at the optimum values. The dependency of phosphate and fluoride ion adsorption by the adsorbent in the presence of competing anions such as SO_4^{2-}, HCO_3^{1-}, and Cl^- (10 and 15 mg L^{-1} each prepared from Na_2SO_4, $NaHCO_3$, and NaCl, respectively) was also evaluated.[37,38] Furthermore, the pH_{pzc} (point of zero charge) of the as-synthesized adsorbent was determined in a separate experiment following a procedure described elsewhere.[39,40]

2.6. Adsorption Isotherm, Kinetics, and Thermodynamics. Adsorption isotherms depict the adsorbates' distribution between the liquid and solid phases with a set of assumptions that include surface heterogeneity or homogeneity, the nature of surface coverage, and the interaction among the adsorbate species. The adsorption isotherms were depicted based on experiments carried out by varying the initial phosphate and fluoride ion concentrations from 10 to 50 ppm keeping the remaining parameters at their optimal values.

Adsorption is a time-dependent phenomenon. It helps to predict the rate and mechanism of adsorption and the adsorbent's ability in eliminating the analytes of interest from the aqueous system. In the present study, typical adsorption kinetic models such as pseudo-first and pseudo-second order were applied for sorption experiments done by varying the contact time as 1, 2, 3, and 6 h keeping all other parameters (pH, adsorbent dose, agitation speed, and initial phosphate and fluoride concentration) at optimized values for a sample volume of 25 mL in each case. The spontaneity of the sorption process was studied at optimized values of the sorption parameters (pH, dosage, contact time, speed of agitation, and initial concentrations) by varying only the temperature as 20, 30, 40, 50, and 60 °C.

2.7. Desorption and Recyclability Studies. To investigate the tendency of phosphate and fluoride ion desorption from the adsorbent, an experiment was conducted on the anion-loaded sorbent. Accordingly, 0.1 g of Ce(III)-BDC MOF powder was placed in each flask containing 25 mL of the desorbing solvents (deionized water and 0.1 M NaOH). After the completion of adsorption, the adsorbate-loaded adsorbent was washed thoroughly with the selected desorbing solvent for 15 min. The recovered material was dried and tested for its adsorptive removal potential for the two analytes without significantly losing its removal capacity for four successive cycles.

3. RESULTS AND DISCUSSION

3.1. XRD Analysis. Ce(III)-BDC MOF was synthesized in aqueous media at ambient temperature. The purity of the phase and crystalline nature of the as-obtained material (Ce(III)-BDC) was examined by XRD (Figure 1). Ce(III)-BDC exhibits remarkable crystallinity without any impurity, as confirmed from the intensity of each of its diffraction peaks. The XRD profile of Ce(III)-BDC was found to be in close agreement with the previously reported Ce-MOFs,[34,41,42] indicating the successful synthesis of Ce(III)-BDC MOF. Also, the XRD patterns of the as-obtained sample prepared at room temperature showed the same reflection as the simulated or theoretical patterns (Figure 1) of $Ce_2(BDC)_6(H_2O)_4$ (CCDC 875876).[34,35] The XRD patterns appeared to be similar before and after the adsorption of the phosphate ion, indicating that the loaded anion does not change the crystalline nature of the material, which can be taken as an advantage for its recyclability.

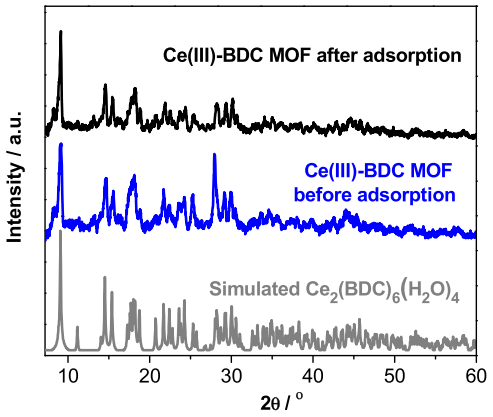

Figure 1. XRD pattern of simulated $Ce_2(BDC)_6(H_2O)_4$ pattern (gray line), and Ce(III)-BDC MOF before (blue) and after adsorption (black) of phosphate ions.

3.2. FTIR Analysis. Figure 2 shows the FTIR spectra of Ce(III)-BDC MOF before and after adsorption. The peak at 3455 cm^{-1} represents the O−H stretching vibrations of

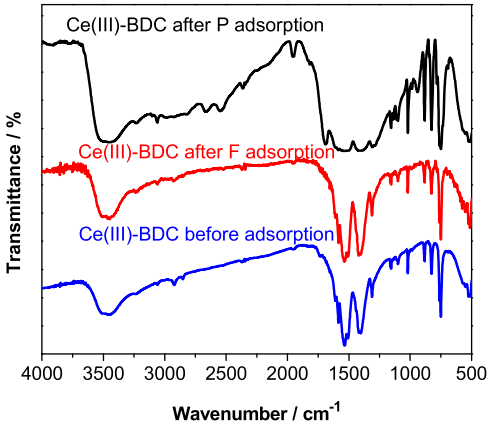

Figure 2. FTIR spectra of Ce(III)-BDC MOF before adsorption (blue line) and after adsorption of fluoride (red) and phosphate (black) ions.

https://doi.org/10.1021/acsomega.3c02290
ACS Omega 2023, 8, 23860−23869

physically adsorbed water. The absorption peak observed at 2918 cm^{-1} indicates the C−H stretching that comes from the linker H_2BDC. The bands at 1538 and 1397 cm^{-1} represent the asymmetric and symmetric vibrations of the carboxylate group, respectively. The weak band observed at 1502 cm^{-1} is associated with the C=C stretching due to the ring, and similar peaks shown at 1411, 823, and 753 cm^{-1} correspond to the C−O stretching of the carboxylate group, C−C bending of the carboxylic group, and O−H bending of the carboxylic group, respectively.[43] Always, a new peak and/or a broader peak observed after adsorption indicates that there is some sort of interaction of the phosphate and fluoride ions with the adsorbent. For example, formation of the inner-sphere complex could be attributed to the phosphate and electrostatic interaction for fluoride adsorption on the adsorbent.[44−46]

3.3. TGA Analysis. The Ce(III)-BDC MOF thermal stability was studied by thermogravimetric analysis (TGA). The thermogravimetric curves of terephthalic acid and Ce(III)-BDC are presented in Figure 3. In the TGA of

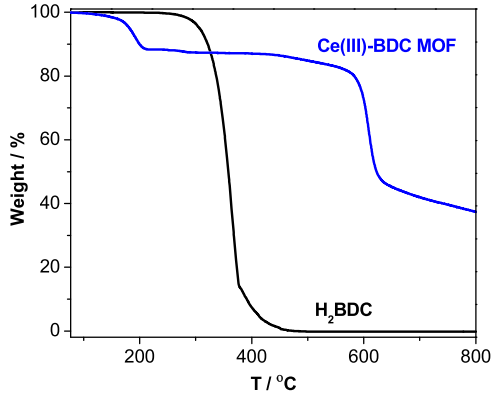

Figure 3. TGA curves of Ce(III)-BDC MOF (blue line) and terephthalic acid (black).

Ce(III)-BDC MOF, the initial weight loss (98−235 °C range, 18.7 wt %) is due to the elimination of free linker (H_2BDC) molecules and/or the coordinated solvent. The second loss (10.4 wt %, up to 570 °C) shows a relatively stable plateau, which is the region of the TGA where the weight is constant, providing the thermal stability information of the sample under the given conditions. The third region showed a larger loss (570−664 °C range, 59.8 wt %), which is attributed to the loss of the terephthalate. In addition to this, the observed temperature range indicates that this Ce(III)-BDC is one of the most stable reported MOFs, much more stable than its homologous Ce(IV)-BDC (UiO-66(Ce)), the stability of which is only around 200 °C.[47] The third mass loss happens at a greater temperature than the decomposition of the linker (370 °C), whose thermal stability is similar to that of Ce-based MOFs prepared from Ce(IV) sources. The residual 40.0 wt % weights obtained for Ce(III)-BDC concur with the value reported previously.[36,47]

3.4. N_2 Sorption Isotherm Analysis. Figure S1 shows the N_2 adsorption/desorption isotherms of the Ce(III)-BDC MOF sample prepared in water as a solvent without any energy input. The BET specific surface area value of the as-obtained Ce(III)-BDC was 15.20 $m^2\ g^{-1}$, three-folds higher than the one reported earlier for the other Ce-based MOFs (5.28 $m^2\ g^{-1}$)[36] and Ce-BDC-2 MOF (1.34 $m^2\ g^{-1}$).[48]

3.5. SEM-EDX Analysis. The SEM micrographs and EDX images of the Ce(III)-BDC MOF before and after phosphate adsorption are presented in Figures 4a,b and S2a,b. In all cases,

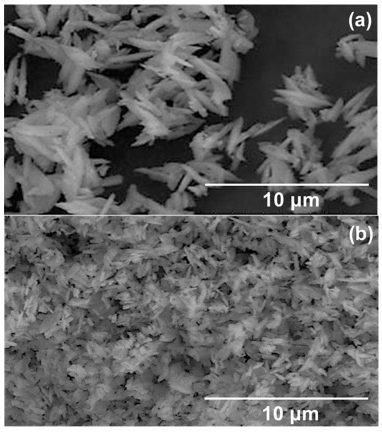

Figure 4. SEM micrographs of Ce(III)-BDC MOF (a) before and (b) after adsorption of phosphate ions.

regular-shaped rice-like particles were clearly observed (Figure 4a) due to the intergrowth of the MOF crystals and homogeneous particles with the average length falling in micrometer (μm) scales. The SEM image and EDX spectrum evidenced the successful synthesis of Ce(III)-MOF from BDC linkers (Figure S2a) and our result concurs with the previous report.[36] The SEM-EDX images of Ce(III)-BDC after adsorption of phosphorus ions revealed some differences due to the adsorption of phosphorus on the Ce(III)-BDC (Figure 4b). Moreover, the EDX spectrum of Ce(III)-BDC MOF before and after adsorption evidenced the presence of the elements of MOF (Figure S2a,b) and also clearly showed that phosphorus was adsorbed onto Ce(III)-BDC (Figure S2b). This is an indication of the potential of Ce(III)-MOF as a good adsorbent for the removal of the target anions from an aqueous solution.

3.6. pH of the Point of Zero Charge (pH_{PZC}). The pH_{pzc} is a parameter that measures the nature of the charge on the adsorbent surface. At pH < pH_{PZC} the adsorbent surface possesses a net positive charge, whereas at pH > pH_{PZC} the surface becomes negatively charged, making the surface ready for adsorbing sorbates with counter charges. In this regard, the target anionic adsorbates will be more attracted to a sorbent surface that is positive.[49] The pH_{PZC} value of the as-obtained MOFs is found to be 4.61 (Figure S3a). From this result, one can infer that the adsorption of both anions on the adsorbent is favored at pH below 4.61.

3.7. Effect of Experimental Parameters. *3.7.1. Effect of pH on Adsorption.* Figure S3b shows the pH effect on phosphate and fluoride ion adsorption. The maximum adsorption was obtained under acidic conditions (pH 3, 4) and showed a decreasing trend when the solution pH was increased. At higher pH, in particular when the pH > pH_{pzc}, the adsorbent surface carried more negative charges, posing a repulsive interaction of the anions (phosphate and fluoride) in solution.[50] The decrease in the adsorption ability at higher pH can be ascribed to the competition for the sorption site between OH^- ions and F^-/PO_4^{3-} ions that have the same charge.[51,52]

3.7.2. Adsorbent Dose and Contact Time Effect. The effect of adsorbent dose on adsorption efficiency is shown in Figure

https://doi.org/10.1021/acsomega.3c02290
ACS Omega 2023, 8, 23860−23869

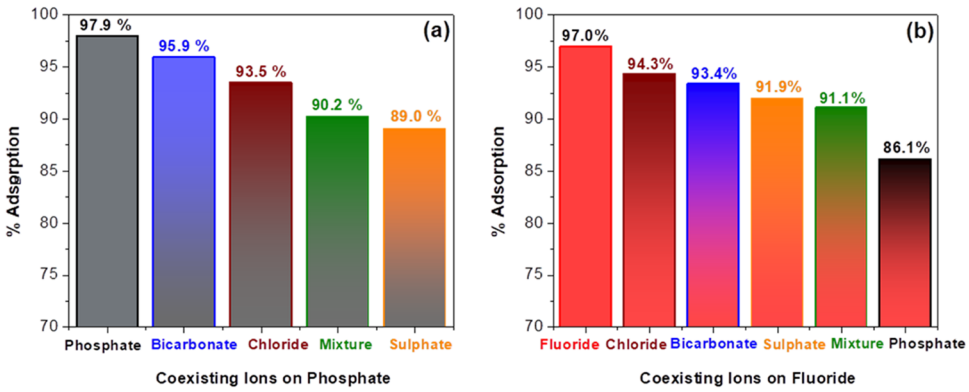

Figure 5. Plot of the effect of coexisting ions: (a) phosphate and (b) fluoride ions (at pH = 3 and 4, adsorbent dose of 0.2 and 0.35 g, concentration of 10 and 15 mg L^{-1}, contact time of 3 and 6 h, and agitation speed of 120 and 100 rpm, respectively).

Table 1. Langmuir and Freundlich Isotherm Constants for Phosphate and Fluoride Adsorption on Ce(III)-BDC MOF

			Langmuir model			Freundlich model		
adsorbent	adsorbate	Q_o	b	R_L	R^2	K_F	n	R^2
Ce(III)-BDC MOF	phosphate	7.4	0.96	0.048	0.984	3.26	1.84	0.947
	fluoride	2.99	0.65	0.068	0.994	1.12	2.22	0.944

S4a. As observed from the plot, the phosphate removal efficiency was enhanced from 77.4 to 99.1% with dose increment from 0.05 to 0.2 g, while the removal efficiency for fluoride increased from 75.1 to 97.2% with dose increment from 0.05 g to 0.35 g. In any case, it must be highlighted that the removal efficiency of Ce(III)-BDC MOF was found to be as high as 99.1 and 97.2% for phosphate and fluoride ions, respectively.

The effect of contact time study on phosphate and fluoride sorption is depicted in Figure S4b. The phosphate and fluoride adsorption by Ce(III)-BDC MOF reached as high as 98.7 and 96.7% at an optimum contact time of 3 and 6 h, respectively. The adsorption rate was faster initially, but reached equilibrium later on. The faster adsorption in the beginning could be due to ample available sites on the adsorbent surface, whereas the decline in the rate of adsorption with increase in time could be due to the limited available adsorption sites. Therefore, the phosphate and fluoride uptake by the adsorbent declined significantly with time due to occupation of the available active sites and possibly due to desorption.[48,53]

3.7.3. Effect of Agitation Speed and Concentration. Figure S5a depicts the influence of speed of agitation on phosphate and fluoride sorption by the adsorbent on varying the speed from 50 to 200 rpm, keeping the rest of the parameters at optimum condition. The efficiency increased with increased agitation speed, reaching a maximum at 120 and 100 rpm with maximum adsorption of 98.8 and 96.7% for phosphate and fluoride, respectively. Increasing the agitation speed further could lead to desorption of the adsorbed anions due to vigorous shaking.[54]

The effect of the initial concentration of both targeted anions on the degree of removal of the adsorbate is exhibited in Figure S5b. This experiment was conducted by varying the initial concentrations of the target ions from 10 to 50 mg L^{-1} keeping the other parameters constant: pH 3 and 4, dose of adsorbent 0.2 and 0.35 g, speed of agitation 120 and 100 rpm, and time of contact 3 and 6 h, respectively. The removal efficiencies of phosphate and fluoride ions by Ce(III)-BDC were found to be 98.2 and 96.4%, respectively. At low concentrations of phosphate and fluoride ions, sufficient numbers of adsorption sites were available on Ce(III)-BDC adsorbents; therefore, most of the phosphate and fluoride ions interacted with the active sites on the adsorbent. With increasing concentrations of the phosphate and fluoride ions in the solution, the removal of the target ions declined due to insufficient number of adsorption sites. Yu and Neretnieks (1990) have also observed a similar trend in this regard.[55] Thus, the initial concentrations of 10 mg L^{-1} for phosphate and 15 mg L^{-1} for fluoride were chosen as optimized values.

3.7.4. Effect of Coexisting Ions. The effect of coexisting ions was assessed for the purpose of detecting the selectivity property of Ce(III)-BDC MOF for the adsorption of phosphate and fluoride anions. Accordingly, the influence of competing ions present in water on phosphate adsorption follows the order SO_4^{2-} > All (mixture) > Cl^- > HCO_3^- (Figure 5a). This trend indicates that phosphate adsorption was influenced more in the presence of sulfate, declining its sorption from 97.9 to 89.0%, whereas HCO_3^- and Cl^- ions interfered less. Such a trend was also shown for the study done on Mg−Al−Fe-based layered double hydroxides.[56] On the other hand, the effect of competing ions on fluoride adsorption was also studied for the as-obtained adsorbent, the results of which followed the order PO_4^{3-} > All (mixture) > SO_4^{2-} > HCO_3^- > Cl^- (Figure 5b). Unlike the phosphate case, the primary interfering ion in fluoride adsorption is phosphate ion, the effect of which is to decrease the percent adsorption from 97.0 to 86.1%. Previous reports revealed a similar trend in this regard.[57] However, the phosphate and fluoride amount adsorbed by the Ce(III)-BDC MOF is considered relatively higher, evidencing the good adsorption capability of the adsorbent in the presence of coexisting ions.

3.8. Adsorption Isotherms. Adsorption isotherm relates the amount adsorbed and its equilibrium concentration in the solution at a constant temperature.[58] The isotherm study was conducted using Langmuir and Freundlich isotherms, the two well-known isotherm models. The results of phosphate and fluoride adsorption isotherms using Ce(III)-BDC MOFs as the sorbent are depicted in Table 1. The Langmuir isotherm model

https://doi.org/10.1021/acsomega.3c02290
ACS Omega 2023, 8, 23860−23869

Table 2. Values of Parameters and Coefficient of Determination of Kinetic Models for Phosphate and Fluoride Adsorption onto Ce(III)-BDC MOF

		adsorbate		pseudo 1st order			pseudo 2nd order		
adsorbent		q_e (mg g^{-1}) exp.	C_o (mg L^{-1})	q_e (mg g^{-1}) calc.	k_1	R^2	q_e(mg g^{-1}) calc.	k_2	R^2
Ce(III)-BDC MOF	phosphate	1.22	10	2.75	1.63	0.89	1.17	4.90	1
	fluoride	0.94	15	2.80	0.56	0.98	0.999	2.80	0.99

Table 3. Calculated Thermodynamic Constants of the Phosphate and Fluoride Adsorption on Ce(III)-BDC MOF

adsorbent	adsorbate	T(K)	ΔG (KJ/mol)	ΔH (KJ/mol)	ΔS (J/mol K)
Ce(III)-BDC MOF	phosphate	303	−3641.2		
		313	−4194.5		
		323	−4747.8	+1312.5	+55.3
		333	−5301		
	fluoride	303	−91.168		
		313	−754.17	+1987.5	+65.9
		323	−1410.2		
		333	−2069.2		

assumes monolayer adsorption onto a surface comprising a limited number of uniform adsorption sites with no interaction among the adsorbates.[59] The linear equation for the Langmuir adsorption model is given as

$$\frac{C_e}{q_e} = \frac{1}{Q_o b} + \frac{C_e}{Q_o} \quad (3)$$

The isotherm's feasibility can be estimated from the dimensionless constant R_L, expressed as

$$R_L = \frac{1}{1 + bC_o} \quad (4)$$

From Table 1, one can easily discern that the R_L values fall between 0 and 1 for favorable adsorption. The Freundlich equation is an empirical equation describing a surface that is heterogeneous with exponential configuration of sites and their energies. The Freundlich isotherm is given by the equation[60]

$$\log q_e = \log K_f + \frac{1}{n} \log C_e \quad (5)$$

The plot C_e/q_e vs C_e provided a straight line with values of 7.43 and 2.99 for Q_o and 0.96 and 0.65 for b for phosphate and fluoride adsorption onto Ce(III)-BDC, respectively (Figure S6a,b). The plot of log q_e vs log C_e resulted in a straight line with values of K_f = 3.26 and 1.12, respectively (Figure S7a,b). Besides, the values of $1/n$ lying between 0 and 1 (0.54 for phosphate and 0.45 for fluoride) yield n values (1.84 and 2.22) falling between 1 and 10, revealing the favorable conditions for the adsorption process.[61] The Langmuir's and Freundlich's plots were interpreted from the correlation coefficient R^2 perspective. Accordingly, the correlation coefficient (R^2) values of the adsorbent in Langmuir's equation are found to be higher than Freundlich's (i.e., 0.984 vs 0.947 and 0.994 vs 0.944 for phosphate and fluoride adsorption on Ce(III)-BDC MOF, respectively, revealing the better fit of the former than the latter). Our finding concurs with the literature reports made previously.[62,63] Moreover, the comparison of the as-obtained Ce(III)-BDC adsorbent with various adsorbents for phosphate and fluoride anion adsorption is presented in Table S1.

3.9. Kinetics of Adsorption. The rate of adsorption and the adsorbate transport mechanism can be estimated from adsorption kinetics study. There are different kinetic models used to interpret the adsorption kinetics. Pseudo-first-order and pseudo-second-order models are the two typical kinetic models. We, therefore, considered these models to evaluate the sorption kinetics of phosphate and fluoride on the as-synthesized cerium-based organic framework.

3.9.1. Pseudo-First-Order Kinetics Model. The pseudo-first-order kinetic model[64] is provided as

$$\log(q_e - q_t) = \log q_e - \frac{K_1}{2.303} t \quad (6)$$

where q_e and q_t are the amounts of phosphate and fluoride ions adsorbed (mg g^{-1}) at equilibrium and at any instant time t (min), respectively. The rate constant k_1 is estimated from the slope of the linear plot of Log($q_e - q_t$) vs t, and q_e is calculated from the intercept of the plot (log q_e = intercept) (Figure S8).

3.9.2. Pseudo-Second-Order Kinetics Model. The pseudo-second-order kinetic model equation[65] is given as

$$\frac{1}{q_t} = \frac{1}{K_2 q_e 2} + \frac{1}{q_e} t \quad (7)$$

where q_e and q_t (mg g^{-1}) are the adsorbed anion amount at equilibrium and at any time t, respectively, k_2 is the adsorption rate constant, t is the contact time (min), k_2 (slope^2/intercept) is obtained by plotting t/q_t vs t based on the above equation, and the value of q_e is 1/slope.

A close agreement between the experimental and calculated values can be predicted based on the coefficient of determination (R^2) and by comparing the calculated q_e vs experimental q_e. R^2 values of 1 and 0.9997 were obtained for the pseudo-second-order kinetic model for phosphate and fluoride ions, respectively. On the other hand, the pseudo-first-order kinetic model resulted in correlation coefficients of 0.89 and 0.98 in that order (Table 2 and Figure S8a,c). We based our study on the pseudo-second order given its better correlation to compare the calculated q_e with its theoretical counterparts. The q_e (calcd) based on pseudo-second-order kinetics was thus found to correspond to 1.17 and 0.99 mg g^{-1} for phosphate and fluoride ions (Figure S8b,d). These values showed close agreement with the experimental data, q_e (exp), listed in Table 2, of 1.22 and 0.94 mg g^{-1} for phosphate and fluoride, respectively. The above result confirms that the mechanism of adsorption by Ce(III)-BDC occurs more via

https://doi.org/10.1021/acsomega.3c02290
ACS Omega 2023, 8, 23860−23869

chemisorption, although other mechanisms such as physisorption cannot be oversighted.

3.10. Thermodynamic Adsorption Study. Thermodynamic entities are all about the spontaneity and feasibility of the adsorption phenomena. The feasibility of a sorption process is predicted by assessing the thermodynamic parameters such as free energy (ΔG), enthalpy (ΔH), and entropy (ΔS). The principal thermodynamic equation relating the above three parameters is as depicted below.[66]

$$\Delta G = \Delta H - T\Delta S \quad (8)$$

where ΔG (KJ/mol), ΔH (KJ mol^{-1}), and ΔS (KJ mol^{-1} K^{-1}) represent the standard free energy change, enthalpy change, and entropy change, respectively, and T is the temperature in Kelvin. The values of ΔH and ΔS could be predicted from the slopes and intercepts of the plot ln K_c vs T^{-1} (Figure S9a,b and Table 3). In addition, based on this plot, the spontaneity of the process can be assessed. K_c calculated from q_e/C_e is the standard thermodynamic equilibrium constant.

The positive enthalpy of sorption for the anions clearly indicates the endothermic nature of the adsorption process that could arise from pore size enlargement and/or activation of the adsorbent surface.[67] The positive values of ΔS indicate the degrees of disorder at the solid solution interface during the adsorption of fluoride and phosphate onto the adsorbent sites.[68,69] On the other hand, the negative ΔG value indicates the spontaneity of the adsorption process (Table 3).

3.11. Desorption Study. Desorption of ions can be calculated from the ratio of the ions desorbed and the total ions adsorbed by the adsorbent. The desorbability of a given ion can, therefore, serve as the degree of fluoride/phosphate desorption from the adsorptive.[70] This experiment was undertaken considering various pH ranging from 2 to 10 (2, 4, 6, 8, and 10) to evaluate the solution pH effect on the desorption of the target ions (Figure S10). According to our results, desorption is favorable at higher pH for both ions. At pH 10, nearly 62.5 and 68.9%, respectively, of the adsorbed phosphate and fluoride ions were released into the liquid regardless of the initial concentration of the target ions used for the batch experiments.

$$\text{desorption efficiency} = \text{desorbed/adsorbed} \times 100 \quad (9)$$

where desorbed refers to the phosphate/fluoride ion concentration after the desorption process and adsorbed = ($C_o - C_e$) for each recovery process.

3.12. Recyclability Study of Ce(III)-BDC MOF. Adsorbent recovery is one of the critical factors influencing the overall efficiency of the adsorption process. An adsorbent is considered economically feasible when it is efficiently regenerated and reused. In this work, the experiment was conducted at pre-optimized conditions and desorption was done using water and 0.1 M NaOH as the desorbent for up to four cycles (Table 4). The adsorption efficiency is highly dependent on the interaction between the adsorbate (phosphate or fluoride anions) and the as-obtained adsorbent.[71,72] The SEM-EDX images evidenced clearly that phosphorus was adsorbed onto Ce(III)-BDC. On the other hand, the −OH group in the adsorbent and fluoride ion (F^-) in the solution could form a Ce−F complex via ligand exchange.[71,73] Furthermore, as a hard acid, Ce^{3+} can easily react with the fluoride ion (F^-) in the solution through electrostatic adsorption and surface complexation,[73] thus realizing fluoride ion removal. The strong interaction between the adsorbent and the target analytes makes the desorption process less effective, warranting further optimization of the solvent employed.[72] Given the strong interaction of the adsorbates, we assumed that the declining efficiency of adsorption in the recycling process might be due to the inadequate washing procedures of the adsorbent material that yielded limited available adsorption sites for the next cycle.

Table 4. Recyclability Study of the Synthesized Sorbent for Phosphate and Fluoride Sorption

analyte	cycle 0	cycle 1	cycle 2	cycle 3	cycle 4
	% removal	% removal	% removal	% removal	% removal
phosphate	97.64	76.00	71.01	61.30	54.75
fluoride	96.00	81.72	72.00	64.59	49.54

4. CONCLUSIONS

The Ce(III)-BDC MOF adsorbent is used to remove phosphate and fluoride ions from an aqueous system. It was synthesized at ambient temperature under sustainable conditions and characterized via techniques such as pH_{pzc}, XRD, FTIR, TGA, and SEM-EDX. The pHpzc for the as-obtained Ce(III)-BDC was found to be 4.61. The XRD results revealed that the expected crystalline phase was obtained with the first reflection scattering angle (2θ) below 10. TGA results affirmed the good thermal stability of the as-obtained Ce(III)-BDC MOFs. FTIR results showed the surface functional group of the adsorbent before and after adsorption of anions. The phosphate and fluoride removal by this adsorbent was efficient (with optimized values above 96%) and it was found to depend on the operating conditions (contact time, adsorbent dosage, agitation speed, pH, coexisting ions, and initial concentration). The adsorption equilibrium is described better by the Langmuir isotherm model, whereas the pseudo-second-order model fits better the sorption kinetics of the as-synthesized sorbent for the target anions. The spontaneity of the sorption process was affirmed by the thermodynamic study. Phosphate and fluoride ion desorption was observed to increase with increasing pH. In addition, the sorbent can be regenerated well for repeated use, implying the adsorbent's potential for environmental application.

■ ASSOCIATED CONTENT

Supporting Information

The Supporting Information is available free of charge at https://pubs.acs.org/doi/10.1021/acsomega.3c02290.

N_2 sorption isotherms of the Ce(III)-BDC MOF; EDX images of this MOF before and after adsorption of phosphate ion; pH of point of zero charge; effect of experimental parameters on the removal of phosphate and fluoride ions (pH, adsorbent dose, contact time, agitation speed, and initial concentration of the target anions), Langmuir and Freundlich adsorption isotherms; kinetics study of adsorption; thermodynamic adsorption of study; desorption study; and comparison of the obtained adsorbent with other adsorbents (PDF)

https://doi.org/10.1021/acsomega.3c02290
ACS Omega 2023, 8, 23860−23869

AUTHOR INFORMATION

Corresponding Authors

Abi M. Taddesse − *Department of Chemistry, Haramaya University, 138 Dire Dawa, Ethiopia*; Phone: +251-912018750; Email: abi92003@yahoo.com

Jemal M. Yassin − *Department of Chemistry, Debre Berhan University, 445 Debre Berhan, Ethiopia*; orcid.org/0000-0002-5638-191X; Phone: +251-912867429; Email: jemalchemistry@gmail.com

Authors

Mitin Belaye − *Department of Chemistry, Haramaya University, 138 Dire Dawa, Ethiopia*

Endale Teju − *Department of Chemistry, Haramaya University, 138 Dire Dawa, Ethiopia*; orcid.org/0000-0003-2455-262X

Manuel Sanchez-Sanchez − *Instituto de Catálisis y Petroleoquímica (ICP), CSIC, 28049 Madrid, Spain*; orcid.org/0000-0002-6592-439X

Complete contact information is available at: https://pubs.acs.org/10.1021/acsomega.3c02290

Notes

The authors declare no competing financial interest.

ACKNOWLEDGMENTS

The authors acknowledge the research grant obtained from Haramaya University (HURG-2016-03-02 and HURG-2020-03-02-75). The authors also acknowledge the Spanish Research Council, CSIC, for funding through the project i-COOP+2018 (COOPA20271). The authors are also indebted to the Institute of Catalysis and Petroleum Chemistry (ICP), Spain, Addis Ababa University and Adama Science and Technology University, for the support afforded to characterize the as-synthesized Ce-MOFs.

REFERENCES

(1) Shannon, M. A.; Bohn, P. W.; Elimelech, M.; Georgiadis, J. G.; Marinas, B. J.; Mayes, A. M. Science and technology for water purification in the coming decades. *Nature* **2008**, *452*, 301−310.

(2) Chong, M. N.; Jin, B.; Chow, C. W.; Saint, C. Recent developments in photocatalytic water treatment technology: a review. *Water Res.* **2010**, *44*, 2997−3027.

(3) Xu, X.; Gao, B.; Jin, B.; Yue, Q. Removal of anionic pollutants from liquids by biomass materials: a review. *J. Mol. Liq.* **2016**, *215*, 565−595.

(4) Han, J.; Kiss, L.; Mei, H.; Remete, A. M.; Ponikvar-Svet, M.; Sedgwick, D. M.; Roman, R.; Fustero, S.; Moriwaki, H.; Soloshonok, V. A. Chemical aspects of human and environmental overload with fluorine. *Chem. Rev.* **2021**, *121*, 4678−4742.

(5) Ruixia, L.; Jinlong, G.; Hongxiao, T. Adsorption of fluoride, phosphate, and arsenate ions on a new type of ion exchange fiber. *J. Colloid Interface Sci.* **2002**, *248*, 268−274.

(6) Ahmad, S.; Singh, R.; Arfin, T.; Neeti, K. Fluoride contamination, consequences and removal techniques in water: a review. *Environ. Sci. Adv.* **2022**, *1*, 620−661.

(7) Hussain, S.; Aziz, H. A.; Isa, M. H.; Ahmad, A.; Van Leeuwen, J.; Zou, L.; Beecham, S.; Umar, M. Orthophosphate removal from domestic wastewater using limestone and granular activated carbon. *Desalination* **2011**, *271*, 265−272.

(8) Nordqvist, M.; Spörndly, R.; Holtenius, K. Faecal excretion of total and acid extractable phosphorus in dairy cows fed rations with different levels of phosphorus. *J. Sci. Food Agric.* **2016**, *96*, 1386−1389.

(9) Guidelines for drinking-water quality. WHO, 2004, https://apps.who.int/iris/bitstream/handle/10665/44584/9789241548151_eng.pdf.

(10) Miretzky, P.; Cirelli, A. F. Fluoride removal from water by chitosan derivatives and composites: a review. *J. Fluor. Chem.* **2011**, *132*, 231−240.

(11) Devi, R. R.; Umlong, I. M.; Raul, P. K.; Das, B.; Banerjee, S.; Singh, L. Defluoridation of water using nano-magnesium oxide. *J. Exp. Nanosci.* **2014**, *9*, 512−524.

(12) Karageorgiou, K.; Paschalis, M.; Anastassakis, G. N. Removal of phosphate species from solution by adsorption onto calcite used as natural adsorbent. *J. Hazard. Mater.* **2007**, *139*, 447−452.

(13) Viswanathan, N.; Meenakshi, S. Role of metal ion incorporation in ion exchange resin on the selectivity of fluoride. *J. Hazard. Mater.* **2009**, *162*, 920−930.

(14) Sehn, P. Fluoride removal with extra low energy reverse osmosis membranes: three years of large scale field experience in Finland. *Desalination* **2008**, *223*, 73−84.

(15) Masomi, M.; Ghoreyshi, A. A.; Najafpour, G. D.; Mohamed, A. R. B. Dynamic adsorption of phenolic compounds on activated carbon produced from pulp and paper mill sludge: experimental study and modeling by artificial neural network (ANN). *Desalin. Water Treat.* **2015**, *55*, 1453−1466.

(16) Wang, S.; Peng, Y. Natural zeolites as effective adsorbents in water and wastewater treatment. *J. Chem. Eng.* **2010**, *156*, 11−24.

(17) Omorogie, M. O.; Agunbiade, F. O.; Alfred, M. O.; Olaniyi, O. T.; Adewumi, T. A.; Bayode, A. A.; Ofomaja, A. E.; Naidoo, E. B.; Okoli, C. P.; Adebayo, T. A.; Unuabonah, E. I. The sequestral capture of fluoride, nitrate and phosphate by metal-doped and surfactant-modified hybrid clay materials. *Chem. Pap.* **2018**, *72*, 409−417.

(18) Yap, M. H.; Fow, K. L.; Chen, G. Z. Synthesis and applications of MOF-derived porous nanostructures. *Green Energy Environ.* **2017**, *2*, 218−245.

(19) Kandiah, M.; Nilsen, M. H.; Usseglio, S.; Jakobsen, S.; Olsbye, U.; Tilset, M.; Larabi, C.; Quadrelli, E. A.; Bonino, F.; Lillerud, K. P. Synthesis and stability of tagged UiO-66 Zr-MOFs. *Chem. Mater.* **2010**, *22*, 6632−6640.

(20) Das, S. K.; Chatterjee, S.; Bhunia, S.; Mondal, A.; Mitra, P.; Kumari, V.; Pradhan, A.; Bhaumik, A. A new strongly paramagnetic cerium-containing microporous MOF for CO_2 fixation under ambient conditions. *Dalton Trans.* **2017**, *46*, 13783−13792.

(21) Ma, S.; Zhou, H.-C. Gas storage in porous metal-organic frameworks for clean energy applications. *Chem. Commun.* **2010**, *46*, 44−53.

(22) Yassin, J. M.; Taddesse, A. M.; Sánchez-Sánchez, M. Sustainable synthesis of a new semiamorphous Ti-BDC MOF material and the photocatalytic performance of its ternary composites with Ag_3PO_4 and g-C_3N_4. *Appl. Surf. Sci.* **2022**, *578*, No. 151996.

(23) Yassin, J. M.; Taddesse, A. M.; Sánchez-Sánchez, M. Sustainable synthesis of semicrystalline Zr-BDC MOF and hetero-structural Ag_3PO_4/Zr-BDC/g-C_3N_4 composite for photocatalytic dye degradation. *Catal. Today* **2022**, *390*−*391*, 162−175.

(24) Hosseini, H.; Ahmar, H.; Dehghani, A.; Bagheri, A.; Fakhari, A. R.; Amini, M. M. Au-SH-SiO_2 nanoparticles supported on metal-organic framework (Au-SH-SiO_2@Cu-MOF) as a sensor for electrocatalytic oxidation and determination of hydrazine. *Electrochim. Acta* **2013**, *88*, 301−309.

(25) Haldoupis, E.; Nair, S.; Sholl, D. S. Efficient calculation of diffusion limitations in metal organic framework materials: a tool for identifying materials for kinetic separations. *J. Am. Chem. Soc.* **2010**, *132*, 7528−7539.

(26) Lawson, H. D.; Walton, S. P.; Chan, C. Metal−organic frameworks for drug delivery: a design perspective. *ACS Appl. Mater. Interfaces* **2021**, *13*, 7004−7020.

(27) Bhattacharjee, S.; Chakraborty, T.; Bhaumik, A. A Ce-MOF as an alkaline phosphatase mimic: Ce-OH_2 sites in catalytic dephosphorylation. *Inorg. Chem. Front.* **2022**, *9*, 5735−5744.

(28) Udourioh, G. A.; Solomon, M.; Matthews-Amune, C. O.; Epelle, E.; Okolie, J.; Agbazue, V. E.; Onyenze, U. Current trends in

https://doi.org/10.1021/acsomega.3c02290
ACS Omega 2023, 8, 23860−23869

the synthesis, characterization and application of Metal-Organic Frameworks. *React. Chem. Eng.* **2023**, *8*, 278−310.
(29) An, J.; Geib, S. J.; Rosi, N. L. Cation-triggered drug release from a porous zinc- adeninate metal-organic framework. *J. Am. Chem. Soc.* **2009**, *131*, 8376−8377.
(30) Zhou, J.; Liu, H.; Lin, Y.; Zhou, C.; Huang, A. Synthesis of well-shaped and high-crystalline Ce-based metal organic framework for CO_2/CH_4 separation. *Microporous Mesoporous Mater.* **2020**, *302*, No. 110224.
(31) Ahmed, I.; Khan, N. A.; Hasan, Z.; Jhung, S. H. Adsorptive denitrogenation of model fuels with porous metal-organic framework (MOF) MIL-101 impregnated with phosphotungstic acid: Effect of acid site inclusion. *J. Hazard. Mater.* **2013**, *250*−*251*, 37−44.
(32) Lin, S.; Song, Z.; Che, G.; Ren, A.; Li, P.; Liu, C.; Zhang, J. Adsorption behavior of metal-organic frameworks for methylene blue from aqueous solution. *Microporous Mesoporous Mater.* **2014**, *193*, 27−34.
(33) Zhai, Y.; Li, Y.; Hou, Q.; Zhang, Y.; Zhou, E.; Li, H.; Ai, S. Highly sensitive colorimetric detection and effective adsorption of phosphate based on MOF-808 (Zr/Ce). *New J. Chem.* **2022**, *46*, 15405−15413.
(34) Zhu, M.; Fu, W.; Zou, G. Urothermal synthesis of an unprecedented pillar-layered metal−organic framework. *J. Coord. Chem.* **2012**, *65*, 4108−4114.
(35) Reineke, T. M.; Eddaoudi, M.; Fehr, M.; Kelley, D.; Yaghi, O. From condensed lanthanide coordination solids to microporous frameworks having accessible metal sites. *J. Am. Chem. Soc.* **1999**, *121*, 1651−1657.
(36) Zheng, Y.; Liu, K.; Qiao, H.; Zhang, Y.; Song, Y.; Yang, M.; Huang, Y.; Guo, N.; Jia, Y.; You, H. Facile synthesis and catalytic properties of CeO_2 with tunable morphologies from thermal transformation of cerium benzendicarboxylate complexes. *CrystEngComm* **2011**, *13*, 1786−1788.
(37) Wambu, E. W.; Kurui, A. J. Fluoride adsorption onto soil adsorbents: the role of pH and other solution parameters. In *Soil pH for Nutrient Availability and Crop Performance*; IntechOpen, 2018.
(38) Liu, R.; Chi, L.; Wang, X.; Wang, Y.; Sui, Y.; Xie, T.; Arandiyan, H. Effective and selective adsorption of phosphate from aqueous solution via trivalent-metals-based amino-MIL-101 MOFs. *Chem. Eng. J.* **2019**, *357*, 159−168.
(39) Mahmood, T.; Saddique, M. T.; Naeem, A.; Westerhoff, P.; Mustafa, S.; Alum, A. Comparison of different methods for the point of zero charge determination of NiO. *Ind. Eng. Chem. Res.* **2011**, *50*, 10017−10023.
(40) Kosmulski, M. The pH dependent surface charging and points of zero charge. IX. Update. *Adv. Colloid Interface Sci.* **2021**, *296*, No. 102519.
(41) Maiti, S.; Dhawa, T.; Mallik, A. K.; Mahanty, S. CeO_2@C derived from benzene carboxylate bridged metal-organic frameworks: ligand induced morphology evolution and influence on the electrochemical properties as a lithium-ion battery anode. *Sustainable Energy Fuels* **2017**, *1*, 288−298.
(42) Zhang, F.; Chen, S.; Nie, S.; Luo, J.; Lin, S.; Wang, Y.; Yang, H. Waste PET as a reactant for lanthanide MOF synthesis and application in sensing of picric acid. *Polymers* **2019**, *11*, No. 2015.
(43) Peng, M. M.; Ganesh, M.; Vinodh, R.; Palanichamy, M.; Jang, H. T. Solvent free oxidation of ethylbenzene over Ce-BTC MOF. *Arab. J. Chem.* **2019**, *12*, 1358−1364.
(44) Raul, P. K.; Devi, R. R.; Umlong, I. M.; Banerjee, S.; Singh, L.; Purkait, M. Removal of fluoride from water using iron oxide-hydroxide nanoparticles. *J. Nanosci. Nanotechnol.* **2012**, *12*, 3922−3930.
(45) Lǔ, J.; Liu, H.; Liu, R.; Zhao, X.; Sun, L.; Qu, J. Adsorptive removal of phosphate by a nanostructured Fe−Al−Mn trimetal oxide adsorbent. *Powder Technol.* **2013**, *233*, 146−154.
(46) Abebe, B.; Taddesse, A. M.; Kebede, T.; Teju, E.; Diaz, I. Fe-Al-Mn ternary oxide nanosorbent: Synthesis, characterization and phosphate sorption property. *J. Environ. Chem. Eng.* **2017**, *5*, 1330−1340.
(47) Yassin, J. M.; Taddesse, A. M.; Sanchez-Sanchez, M. Room temperature synthesis of high-quality Ce (IV)-based MOFs in water. *Microporous Mesoporous Mater.* **2021**, *324*, No. 111303.
(48) He, J.; Pei, C.; Yang, Y.; Lai, B.; Sun, Y.; Yang, L. The structural design and valence state control of cerium-based metal-organic frameworks for their highly efficient phosphate removal. *J. Clean. Prod.* **2021**, *321*, No. 128778.
(49) Srivastava, V. C.; Mall, I. D.; Mishra, I. M. Adsorption of toxic metal ions onto activated carbon: Study of sorption behaviour through characterization and kinetics. *Chem. Eng. Process.* **2008**, *47*, 1269−1280.
(50) Cai, P.; Zheng, H.; Wang, C.; Ma, H.; Hu, J.; Pu, Y.; Liang, P. Competitive adsorption characteristics of fluoride and phosphate on calcined Mg−Al−CO_3 layered double hydroxides. *J. Hazard. Mater.* **2012**, *213*, 100−108.
(51) Fawell, J.; Bailey, K.; Chilton, J.; Dahi, E.; Magara, Y. *Fluoride in Drinking-Water*; IWA Publishing, 2006.
(52) Shimelis, B.; Zewge, F.; Chandravanshi, B. S. Removal of excess fluoride from water by aluminum hydroxide. *Bull. Chem. Soc. Ethiop.* **2006**, *20*, 17−34.
(53) Yadav, A. K.; Kaushik, C.; Haritash, A. K.; Kansal, A.; Rani, N. Defluoridation of groundwater using brick powder as an adsorbent. *J. Hazard. Mater.* **2006**, *128*, 289−293.
(54) Namasivayam, C.; Sangeetha, D. Equilibrium and kinetic studies of adsorption of phosphate onto $ZnCl_2$ activated coir pith carbon. *J. Colloid Interface Sci.* **2004**, *280*, 359−365.
(55) Yu, J. W.; Neretnieks, I. Single-component and multi-component adsorption equilibria on activated carbon of methyl-cyclohexane, toluene, and isobutyl methyl ketone. *Ind. Eng. Chem. Res.* **1990**, *29*, 220−231.
(56) Jia, Z.; Hao, S.; Lu, X. Exfoliated Mg−Al−Fe layered double hydroxides/polyether sulfone mixed matrix membranes for adsorption of phosphate and fluoride from aqueous solutions. *J. Environ. Sci.* **2018**, *70*, 63−73.
(57) Suneetha, M.; Sundar, B. S.; Ravindhranath, K. Removal of fluoride from polluted waters using active carbon derived from barks of Vitex negundo plant. *J. Anal. Sci. Technol.* **2015**, *6*, No. 15.
(58) Karthikeyan, G.; Ilango, S. S. Fluoride sorption using Morringa Indica-based activated carbon. *J. Environ. Health Sci. Eng.* **2007**, *4*, 21−28.
(59) Halajnia, A.; Oustan, S.; Najafi, N.; Khataee, A.; Lakzian, A. Adsorption−desorption characteristics of nitrate, phosphate and sulfate on Mg−Al layered double hydroxide. *Appl. Clay Sci.* **2013**, *80*, 305−312.
(60) Foo, K. Y.; Hameed, B. H. Insights into the modeling of adsorption isotherm systems. *J. Chem. Eng.* **2010**, *156*, 2−10.
(61) Viswanathan, N.; Sundaram, C. S.; Meenakshi, S. Sorption behaviour of fluoride on carboxylated cross-linked chitosan beads. *Colloids Surf., B* **2009**, *68*, 48−54.
(62) Kumar, E.; Bhatnagar, A.; Ji, M.; Jung, W.; Lee, S.-H.; Kim, S.-J.; Lee, G.; Song, H.; Choi, J.-Y.; Yang, J.-S.; Jeon, B. H. Defluoridation from aqueous solutions by granular ferric hydroxide (GFH). *Water Res.* **2009**, *43*, 490−498.
(63) Tofik, A.; Taddesse, A. M.; Tesfahun, K.; Girma, G. Fe−Al binary oxide nanosorbent: Synthesis, characterization and phosphate sorption property. *J. Environ. Chem. Eng.* **2016**, *4*, 2458−2468.
(64) Ho, Y.-S.; McKay, G. Kinetic models for the sorption of dye from aqueous solution by wood. *Process Saf. Environ. Prot.* **1998**, *76*, 183−191.
(65) Hamadi, N. K.; Chen, X. D.; Farid, M. M.; Lu, M. G. Adsorption kinetics for the removal of chromium (VI) from aqueous solution by adsorbents derived from used tyres and sawdust. *J. Chem. Eng.* **2001**, *84*, 95−105.
(66) Rodrigues, L. A.; da Silva, M. L. C. P. An investigation of phosphate adsorption from aqueous solution onto hydrous niobium oxide prepared by co-precipitation method. *Colloids Surf. A: Physicochem. Eng.* **2009**, *334*, 191−196.
(67) Yan, L.-g.; Xu, Y.-y.; Yu, H.-q.; Xin, X.-d.; Wei, Q.; Du, B. Adsorption of phosphate from aqueous solution by hydroxy-

https://doi.org/10.1021/acsomega.3c02290
ACS Omega 2023, 8, 23860−23869

aluminum, hydroxy-iron and hydroxy-iron−aluminum pillared bentonites. *J. Hazard. Mater.* **2010**, *179*, 244−250.
(68) Sundaram, C. S.; Viswanathan, N.; Meenakshi, S. Fluoride sorption by nano-hydroxyapatite/chitin composite. *J. Hazard. Mater.* **2009**, *172*, 147−151.
(69) Anirudhan, T. S.; Senan, P. Adsorption of phosphate ions from water using a novel cellulose-based adsorbent. *Chem. Ecol.* **2011**, *27*, 147−164.
(70) Zeng, L.; Li, X.; Liu, J. Adsorptive removal of phosphate from aqueous solutions using iron oxide tailings. *Water Res.* **2004**, *38*, 1318−1326.
(71) Zhou, Z.; Li, D.; Huang, W.; Wang, R.; Zhong, J.; Zhang, Y.; Meng, J.; Li, C. Phosphate adsorption on cerium/terephthalic acid Metal−Organic Frameworks (Ce-MOF) driven by effective electrostatic attraction and ligand exchange in a wide pH range. *Chem. Asian J.* **2023**, No. e202300202.
(72) Wang, Y.; Xie, X.; Chen, X.; Huang, C.; Yang, S. Biochar-loaded Ce^{3+}-enriched ultra-fine ceria nanoparticles for phosphate adsorption. *J. Hazard. Mater.* **2020**, *396*, No. 122626.
(73) Song, J.; Yang, W.; Han, X.; Jiang, S.; Zhang, C.; Pan, W.; Jian, S.; Hu, J. Performance of Rod-Shaped Ce Metal−Organic Frameworks for Defluoridation. *Molecules* **2023**, *28*, No. 3492.

https://doi.org/10.1021/acsomega.3c02290
ACS Omega 2023, 8, 23860−23869